Multipolar edge states in the anisotropic kagome antiferromagnet

Judit Romhányi*
Okinawa Institute of Science and Technology Graduate University, Onna-son, Okinawa 904-0395, Japan

(Received 3 October 2018; published 9 January 2019)

Excitations of ordered insulating magnets gain renewed interest due to their potential topological properties and the natural realization of magnetic analogues of the celebrated topological models. Here, we study the topologically nontrivial multiplet excitations of the spin-1/2 kagome antiferromagnet with strong breathing anisotropy and Dzyaloshinskii-Moriya interaction. We show that in the chiral magnetic ground state the excitations can be characterized with a spin-1/2 doublet and a spin-3/2 quartet. Applying magnetic field, we can tune a band touching topological transition within the quartet band. At the transition point a spin-3/2 Dirac cone is formed by the touching of four bands. In the topologically nontrivial regime the spin-3/2 bands have large Chern numbers -3, -1, 1, 3. Furthermore, the chiral edge states appearing for open boundary condition naturally inherit the multipolar characters and we find novel quadrupolar edge modes.

DOI: 10.1103/PhysRevB.99.014408

I. TOPOLOGICAL MAGNETIC EXCITATIONS

Since the discovery of quantum Hall effect the concept of topology has rapidly spread from itinerant electron systems to a wider scope including bosonic excitations. In addition to the Hall effect of photonic crystals [1–6], phonon modes [7–9], and skyrmion textures [10–12], the topological properties of magnetic excitations in insulating quantum magnets continues to attain growing interest. The topological Haldane model realized naturally in the magnon spectrum of iron-based honeycomb insulators [13] and the Weyl magnons emerging in breathing pyrochlore lattice [14] illustrate well the advances of magnetic analogues of topological electron bands.

Topological band structure of magnons in insulating kagome ferromagnet has been predicted theoretically [15] and found in experiments [16]; furthermore Weyl magnon nodes have been reported in stacked kagome antiferromagnets in Ref. [17]. The theoretical prediction of Hall effect of topologically nontrivial triplet excitations [18,19] and the experimental observation of topologically protected chiral edge modes in the orthogonal dimer system, $SrCu_2(BO_3)_2$ [20], opened a route to generalization of topological magnons. Expanding this idea, we propose that two-dimensional quantum magnets with breathing anisotropy can exhibit topologically nontrivial multiplet excitations similar to the triplets observed in $SrCu_2(BO_3)_2$. Considering a cluster of spins, the local Hilbert space is enlarged, encompassing higher multipole degrees of freedom. A plaquette of three $S = 1/2$ quantum spins, for example, gives room for an effective spin-3/2 quartet, the next multiplet after the spin-1 triplet of the dimerized system.

We propose that unconventional excitations of ordered quantum magnets cannot only hold similar properties to the topological electron bands but can offer a new playground for multipolar topological bands arising naturally as a consequence of quantum mechanical entanglement between magnetic degrees of freedom. To illustrate this, we study the spin-1/2 kagome antiferromagnet with breathing anisotropy in the framework of weakly interacting trimers. Keeping the triangular building blocks entangled, the excitation spectrum includes propagating multiplets. When the $S = 3/2$ quartet excitations have nontrivial topology, due to their multiplet character, they exhibit large Chern numbers and corresponding multipolar edge states.

II. MODEL HAMILTONIAN

We consider the trimerized kagome antiferromagnet with intratrimer Dzyaloshinskii-Moriya (DM) anisotropy and magnetic field perpendicular to the lattice plane. Figure 1 illustrates the breathing kagome lattice together with the magnetic and coinciding crystallographic unit cell. The Hamiltonian is given by Eq. (1).

$$\mathcal{H} = J \sum_{i,j\in\Delta} \boldsymbol{S}_i \cdot \boldsymbol{S}_j + J' \sum_{i,j\in\nabla} \boldsymbol{S}_i \cdot \boldsymbol{S}_j + D \sum_{i,j\in\Delta} (\boldsymbol{S}_i \times \boldsymbol{S}_j)_z - g_z h^z \sum_i S_i^z \,. \tag{1}$$

When J is large compared to J', considering entangled strong up-triangles as the elementary unit is well justified. As a first step we construct the basis for the weakly interacting trimers by diagonalizing the eight-dimensional local Hilbert space of a single triangle. The SU(2) symmetry splits this basis into two four-dimensional subspaces as $\mathcal{D}^{(\frac{1}{2})} \otimes \mathcal{D}^{(\frac{1}{2})} \otimes \mathcal{D}^{(\frac{1}{2})} = 2\mathcal{D}^{(\frac{1}{2})} \oplus \mathcal{D}^{(\frac{3}{2})}$. Therefore, when spin rotational symmetry is preserved, and in case of antiferromagnetic exchange, the spectrum of a single triangle consists of two degenerate low-lying spin-1/2 doublets and a high-energy spin-3/2 quartet.

Taking the intratrimer DM interaction depicted in Fig. 1 into account, we can further split the spectrum. The uniform z component of the intertrimer DM interaction correspond,

*Corresponding author: judith.romhanyi@gmail.com

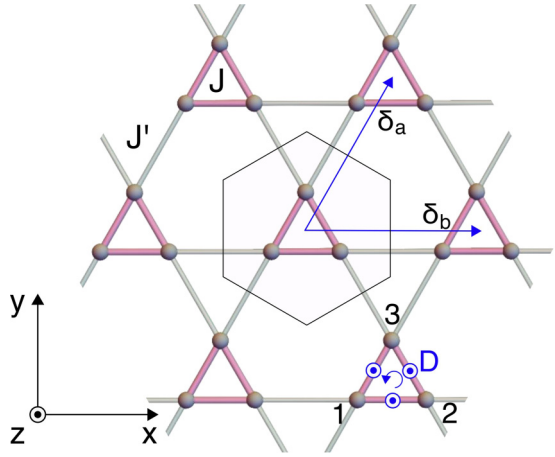

FIG. 1. Breathing kagome lattice with Heisenberg and DM couplings. The intratrimer DM vector $\mathbf{D} = (0, 0, D)$ is pointing in or out of the lattice plane on each bond as we go around the strong up-triangles indicated by blue arrow. The coinciding structural and magnetic unit cell is shown by a hexagon, together with the lattice translation vectors δ_a and δ_b.

in fact, to the z component of the vector chirality:

$$\chi_v = \frac{2}{3\sqrt{3}}(\boldsymbol{S}_1 \times \boldsymbol{S}_2 + \boldsymbol{S}_2 \times \boldsymbol{S}_3 + \boldsymbol{S}_3 \times \boldsymbol{S}_1). \tag{2}$$

The z component of DM lowers the spin rotation symmetry to U(1), and the low-lying doublets split as D selects a specific chirality. The nonchiral $S = \frac{3}{2}$ states remain unaffected by the DM coupling. We use the total spin of the trimer S, its z component S^z, and the z component of the vector chirality χ_v^z to distinguish the states and introduce the notation $|S, m, \chi_v^z\rangle$ to label them. Similar chiral basis has been considered in Ref. [21]. Details of the multiplet basis are given in Appendix A and Fig. 2 illustrates the level scheme.

The strength of the DM interaction determines the gap between the low-lying doublets and the breathing anisotropy; J/J' is responsible for the gap between the quartet and the doublets. Here, we consider larger breathing and DM anisotropies to have well separated multiplets that barely mix with each other. This allows us to construct simple effective

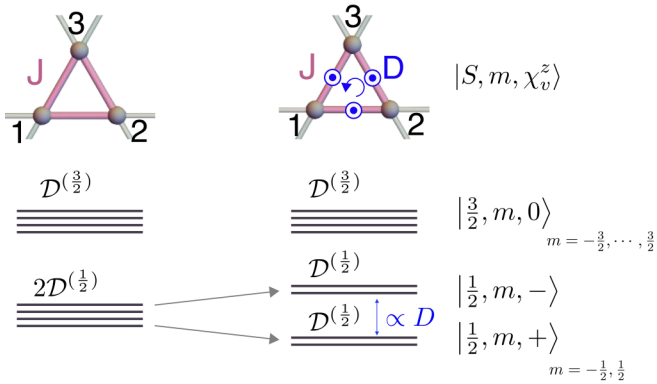

FIG. 2. Level scheme of a triangle. Including the DM interaction, the chiral doublets split. Depending on the sign of D, the doublet with positive or with negative chirality is lowered. We choose $D < 0$, which lowers the $|\frac{1}{2}, \pm\frac{1}{2}, +\rangle$.

hopping models describing the multiplets' dynamics. The advantage of the effective picture is that it gives a simple interpretation for the topological properties of the multiplets which we discuss in Secs. III B and III C in detail.

Smaller anisotropies decrease the gaps that separate the multiplets and the perturbative approach becomes less accurate. To be able to characterize the ground state and excitations for a more isotropic case too, we need to use multiboson spin wave calculations that can describe all the multiplet excitations on an equal footing and can take the mixing between the multiplets into account. This method is valid for a wider range of parameters, however, the simple physical picture given by the effective model for the characterization of the topology of bands is lost. Nonetheless, we validate our effective model computing the multiboson spectrum from the anisotropic case in Appendix E and compare them with the results of the effective model describing the well separated spin multiplets.

III. EFFECTIVE MODEL FOR THE ANISOTROPIC MODEL

A. Ground state and the lowest excitation

Let us consider the anisotropic case and well separated multiplets. In the following, we fix the sign of D to be negative. The spectrum of the isolated triangles can be divided into three parts: A large gap ($\sim\frac{3J}{2}$) separates the nonchiral quartet and the chiral doublet manifolds, furthermore the DM interaction shifts the spin-half states with positive and negative chirality into the opposite direction: $D < 0$ lowers the energy of states with positive chirality, $|S, m, \chi_v^z\rangle = |\frac{1}{2}, \pm\frac{1}{2}, +\rangle$. These are degenerate when the magnetic field is zero and form the lowest lying subspace as shown in Fig. 2. Taking the intertrimer coupling J' into account, the $\pm\frac{1}{2}$ states become mixed to minimize the energy of the intertrimer bonds. We write the new basis for the lowest-lying doublet as

$$\begin{aligned} |\mathcal{A}\rangle &= \cos\vartheta \left|\tfrac{1}{2}, \tfrac{1}{2}, +\right\rangle + e^{i\varphi} \sin\vartheta \left|\tfrac{1}{2}, -\tfrac{1}{2}, +\right\rangle \\ |\mathcal{B}\rangle &= \sin\vartheta \left|\tfrac{1}{2}, \tfrac{1}{2}, +\right\rangle - e^{i\varphi} \cos\vartheta \left|\tfrac{1}{2}, -\tfrac{1}{2}, +\right\rangle, \end{aligned} \tag{3}$$

where the parameter φ can take arbitrary value reflecting the remaining U(1) symmetry. For convenience, we choose $\varphi = -\frac{5\pi}{6}$, so that in the ground state the spins are pointing all out on the up-triangles (and all in for the orthogonal state). $\vartheta = \frac{1}{2}\arccos\frac{g_z h^z}{J'}$ is obtained by minimizing the ground state energy,

$$E_0 = -\frac{3J}{4} + \frac{\sqrt{3}D}{2} - \frac{J'(1 - 3\cos 4\vartheta)}{24} - \frac{g_z h^z \cos 2\vartheta}{2}. \tag{4}$$

The parameter ϑ determines how much the spins are tilting out of the plane towards the magnetic field.

When the field is zero, $\vartheta = \frac{\pi}{4}$, and the $\pm\frac{1}{2}$ states mix equally to form a planar 120° type of order. A finite magnetic field cants the spins uniformly out of the plane and a chiral magnetic 'umbrella' state is realized as the ground state. Let us note that the ground state is not the classical planar or canted 120° state. The trimers are entangled which is manifested in the shorter spin length;

$$\langle\mathcal{A}|\boldsymbol{S}_n|\mathcal{A}\rangle = R_z\left(n\frac{2\pi}{3}\right)\left(0, \frac{1}{3}\sin 2\vartheta, \frac{1}{6}\cos 2\vartheta\right), \tag{5}$$

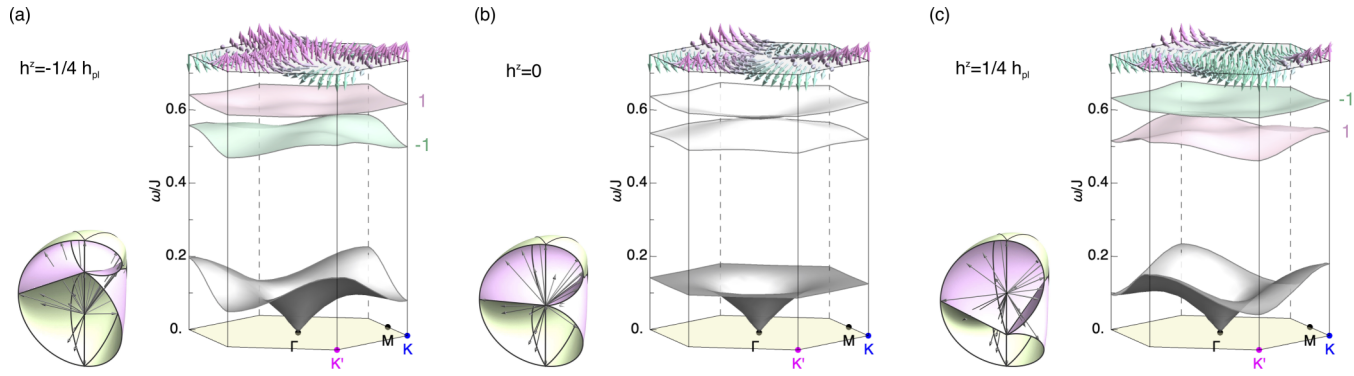

FIG. 3. Topological bands of the doublet subspace. The lowest topologically trivial mode corresponding to the propagation of $|\text{all-in}\rangle$ and given by $\omega_{\mathbf{k}}$ of Eq. (7) is displayed in gray color. (a) At $h_{\rm pl} < h^z < 0$ fields the doublet excitations are nondegenerate and the Chern number is well defined taking the values -1, 1. The pseudomagnetic field $\boldsymbol{d}_{\mathbf{k}}$ forms a skyrmion in the hexagonal BZ as illustrated above the dispersions. Drawing these vectors in a common origin, they map out a surface plotted next to the bands. For better visualization we cut these surfaces in half, so that one can see inside. When the origin is enclosed in the surface, the topology of the doublet is nontrivial. (b) At $h^z = 0$ the gap closes at the Γ point, indicating that $\mathbf{d}_\Gamma = \mathbf{0}$, and the origin is on the surface between the chambers. The flux of the $\boldsymbol{d}_{\mathbf{k}}$ is zero. (c) For $h^z > 0$, the gap opens again, the origin moves to the upper chamber of the surface, and the topology of the doublets is reversed with the reversed flux of the pseudomagnetic field $\boldsymbol{d}_{\mathbf{k}}$ illustrated above the dispersion. More information on the skyrmions of $\boldsymbol{d}_{\mathbf{k}}$ can be found in Appendix D ($J = 1$, $J' = 0.2$, $D_z = -0.3$, and $g_z = 2$).

with $n = 1, 2, 3$ denoting the sites of the triangle and the operator $R_z(\alpha)$ corresponding to a real α rotation about the z axis. The spin expectation value for the orthogonal all-in state $|\text{all-in}\rangle$ differs only in sign. We note that J' couples the lowest all-in all-out subspace to the states $|3/2, \pm 3/2, 0\rangle$, too. However, the mixing with the 3/2 multiplet is second order in J'/J and negligible compared to the mixing within the spin-half subspace.

At a trimer-product level, the ground state is the realization of $|\text{all-in}\rangle$ on each strong triangle of the breathing lattice. We project the full Hamiltonian (1) onto the lowest-lying subspace and treat $|\text{all-in}\rangle$ and $|\text{all-out}\rangle$ as the two components of a pseudo-spin-half. Using conventional linear spin wave theory, we calculate the lowest excitation which can be thought of as 'flipping' a pseudospin, i.e., removing a state $|\text{all-in}\rangle_j$ and creating $|\text{all-out}\rangle_j$. Such a local excitation can propagate over the lattice via J' to gain kinetic energy. We introduce a boson for this excitation: $|\text{all-out}\rangle_j = a_j^\dagger|0\rangle$, where the vacuum state, $|0\rangle$, corresponds to the condensation of $|\text{all-in}\rangle$. The spin wave Hamiltonian has the following form

$$\mathcal{H}^{\rm sw} = \begin{pmatrix} a_{\mathbf{k}}^\dagger \\ a_{-\mathbf{k}} \end{pmatrix} \begin{pmatrix} M_{\mathbf{k}} & N_{\mathbf{k}} \\ N_{-\mathbf{k}}^* & M_{-\mathbf{k}}^* \end{pmatrix} \begin{pmatrix} a_{\mathbf{k}} \\ a_{-\mathbf{k}}^\dagger \end{pmatrix}, \tag{6}$$

with $M_{\mathbf{k}} = \frac{J'}{6}[4 - (1 + \frac{3(g_z h^z)^2}{J'^2})\gamma_1] + \frac{2\sqrt{3}}{3} g_z h^z \gamma_2$ and $N_{\mathbf{k}} = \frac{J'}{2}[1 - \frac{(g_z h^z)^2}{J'^2}]\gamma_1$. Equation (6) is diagonalized using Bogoliubov transformation. The dispersion of the resulting mode is given by

$$\omega_{\mathbf{k}} = \frac{J'}{3}\sqrt{2(1-\gamma_1)\left[(2+\gamma_1) - \frac{3(g_z h^z)^2}{J'^2}\right]} + \frac{2\sqrt{3}}{3} g_z h^z \gamma_2 \tag{7}$$

and is shown in Fig. 3. The geometrical factors are

$$\gamma_1 = \frac{1}{3}\sum_{n=1}^{3} \cos \boldsymbol{k}\cdot\boldsymbol{\delta}_n \quad \text{and} \quad \gamma_2 = \frac{1}{3}\sum_{n=1}^{3} \sin \boldsymbol{k}\cdot\boldsymbol{\delta}_n, \tag{8}$$

where $\boldsymbol{\delta}_n$ takes the values $\boldsymbol{\delta}_1 = \boldsymbol{\delta}_b - \boldsymbol{\delta}_a = (-1/2, \sqrt{3}/2)$, $\boldsymbol{\delta}_2 = \boldsymbol{\delta}_a = (1/2, \sqrt{3}/2)$, and $\boldsymbol{\delta}_3 = -\boldsymbol{\delta}_b = (-1, 0)$ as introduced in Fig. 1. Equation (6) is derived in Appendix A.

Increasing the magnetic field to $h_{\rm pl} = \pm J'/g_z$, $\omega_{\mathbf{k}}$ softens quadratically at the K/K' point of the Brillouin zone (BZ) and a phase transition takes place from the chiral state into a gapped uniform 1/3-plateau phase above $h_{\rm pl}$. The plateau phase is characterized by $\vartheta = 0$, $\boldsymbol{S}_j = (0, 0, \frac{1}{6})$ and the condensation of $|\frac{1}{2}, -\frac{1}{2}, +\rangle$ state on each up-triangle. A variational phase diagram taking into account the full eight-dimensional Hilbert space of the trimer is provided in the Appendix E supporting the phase transition to the plateau phase at $h_{\rm pl} = \pm J'/g_z$ in case of stronger breathing and DM anisotropies.

B. Topology of multiplet excitations

The remaining six orthogonal states, the doublet with negative chirality, $|\frac{1}{2}, m, -\rangle$, and the nonchiral quartet, $|\frac{3}{2}, m, 0\rangle$, comprise the gapped excitations. The multiplet dynamics in leading order in J'/J is characterized by hopping processes such as

$${}_i\langle \tfrac{1}{2}, m, -|\mathcal{H}|\tfrac{1}{2}, m', -\rangle_j \quad \text{and} \quad {}_i\langle \tfrac{3}{2}, m, 0|\mathcal{H}|\tfrac{3}{2}, m', 0\rangle_j, \tag{9}$$

where the site indices i and j are either the same or belong to neighboring up-triangles, and m and m' can take the values $-S, \ldots, S$, for $S = \frac{1}{2}$ and $\frac{3}{2}$.

Introducing bosonic operators $|\frac{1}{2}, m, -\rangle_j = b_{m,j}^\dagger|0\rangle$ and $|\frac{3}{2}, m, 0\rangle_j = c_{m,j}^\dagger|0\rangle$ for the two multiplets, we calculate the hopping matrix elements as detailed in the Appendices B and C. After Fourier transformation, the effective Hamiltonians are obtained in the form of

$$\mathcal{H}^{(1/2)} = \sum_k \sum_{mm'} b_{m,\mathbf{k}}^\dagger B_{mm'}(\mathbf{k}) b_{m',\mathbf{k}} \quad \text{and}$$
$$\mathcal{H}^{(3/2)} = \sum_k \sum_{mm'} c_{m,\mathbf{k}}^\dagger C_{mm'}(\mathbf{k}) c_{m',\mathbf{k}}, \tag{10}$$

where $B_{mm'}(\mathbf{k})$ and $C_{mm'}(\mathbf{k})$ are $2S+1$-dimensional matrices with $S=1/2$ and $3/2$, respectively. We can rewrite the hopping matrices in the convenient form

$$B(\mathbf{k}) = \Delta_{\mathbf{k}}^{(1/2)} \cdot \mathbf{1}_2 + \boldsymbol{d}_{\mathbf{k}}^{(1/2)} \cdot \boldsymbol{s} \quad \text{and} \tag{11a}$$

$$C(\mathbf{k}) = \Delta_{\mathbf{k}}^{(3/2)} \cdot \mathbf{1}_4 + \boldsymbol{d}_{\mathbf{k}}^{(3/2)} \cdot \boldsymbol{S}, \tag{11b}$$

where $\mathbf{1}_n$ is an n-dimensional unit matrix, $\Delta_{\mathbf{k}}^{(S)}$ is a shift in the energy corresponding to the gap and $\boldsymbol{d}_{\mathbf{k}}^{(S)}$ is a pseudomagnetic field that induces a Zeeman-like splitting of the S multiplets. For the $S=1/2$ subspace, the vector $\boldsymbol{s}$ simply contains the three Pauli matrices, $\frac{1}{2}\boldsymbol{\sigma}$, while for the quartet, $\boldsymbol{S}$ corresponds to the x, y, z components of a spin-3/2 quantum spin.

In case of the doublet, obtaining the simple form of $\Delta_{\mathbf{k}}^{(1/2)} \cdot \mathbf{1}_2 + \boldsymbol{d}_{\mathbf{k}}^{(1/2)} \cdot \boldsymbol{s}$ is obvious, as the operator space of a quantum spin-1/2 is four dimensional, and $\boldsymbol{s}$ together with $\mathbf{1}_2$ form a basis for it. This argument breaks down in the case of the quartet, as the operator space is 16 dimensional, including seven octupole and five quadrupole operators beside the spin components $\boldsymbol{S}$ and the identity operator $\mathbf{1}_4$ which contribute to the dynamics of the quartet. The reason is that the original Hamiltonian (1) contains only spin-spin interactions, and higher order, quadrupole-quadrupole or octupole-octupole terms are not present.

Naturally, both $\boldsymbol{s}$ and $\boldsymbol{S}$ satisfy SU(2) algebra. Therefore, we can think about the multiplets as a spin-S object in momentum space that is coupled to the pseudomagnetic field $\boldsymbol{d}_{\mathbf{k}}^{(S)}$. Diagonalizing Eqs. (11) the eigenvalue of the mth band in the S multiplet has the form $\omega_m(\mathbf{k}) = \Delta_{\mathbf{k}}^{(S)} + m \cdot d_{\mathbf{k}}^{(S)}$, with $d_{\mathbf{k}}^{(S)} = |\boldsymbol{d}_{\mathbf{k}}^{(S)}|$.

It is apparent that when $\boldsymbol{d}_{\mathbf{k}}^{(S)}$ vanishes at some point in the BZ, the bands with different m touch at a single point. In case of the quartet, this corresponds to a novel spin-3/2 Dirac cone, with four bands touching at the transition point between topologically trivial and nontrivial phases. When $\boldsymbol{d}_{\mathbf{k}}^{(S)}$ is finite everywhere in the BZ, the multiplets are split and their topological properties can be characterized by a well-defined Chern number. The pseudomagnetic field, $\boldsymbol{d}_{\mathbf{k}}^{(S)}$, carries all the information on the topology. When the bands are topologically nontrivial, $\boldsymbol{d}_{\mathbf{k}}^{(S)}$ forms a skyrmion in the BZ as illustrated above the dispersions in Figs. 3 and 4. The skyrmion number N_S is closely related to the Chern number of the bands [18]. For magnetic fields $h>0$ the Chern number is $C_m^{(3/2)} = 2mN_S$ with $m=-3/2,\ldots,3/2$ for the $S=3/2$ multiplet and $C_m^{(1/2)} = -2mN_S$ for the $S=1/2$ doublet with $m=-1/2, 1/2$. Changing the direction of the field, the Chern numbers switch signs.

We can use the magnetic field as a tuning parameter to change the topological properties of the bands. At zero field, both $\boldsymbol{d}_{\mathbf{k}}^{(1/2)}$ and $\boldsymbol{d}_{\mathbf{k}}^{(3/2)}$ vanish at the Γ point, and the bands touch in both the spin-1/2 and spin-3/2 subspaces. Turning the magnetic field on, the bands acquire topologically nontrivial characters without changing the chiral magnetic ground state as long as $h^z < h_{\mathrm{pl}}$.

We can formulate the topological properties using geometry. Drawing the $\boldsymbol{d}_{\mathbf{k}}^{(S)}$ vectors in a common origin, they map out a two-dimensional surface. When the origin, a monopole for Berry phase, is enclosed in the surface, the bands are topologically nontrivial, and when it is outside of the surface they are trivial. If $\boldsymbol{d}_{\mathbf{k}}^{(S)} = \mathbf{0}$ at a given point in the BZ, the origin is a point of the surface and the multiplet excitations are degenerate.

The Dirac-like physics of the lower doublet excitations is shown in Fig. 3. The dispersion of the spin-1/2 bands, $\omega_{\mathbf{k}}^{(1/2)} = \Delta^{(1/2)} \pm 1/2 \cdot d_{\mathbf{k}}^{(1/2)}$, along with the surface formed by $\boldsymbol{d}_{\mathbf{k}}^{(1/2)}$ is shown for different values of magnetic field. Above the dispersion we plot the skyrmion formed by the pseudofield $\boldsymbol{d}_{\mathbf{k}}^{(1/2)}$. The $\boldsymbol{d}_{\mathbf{k}}^{(1/2)}$ and $\Delta_{\mathbf{k}}^{(1/2)}$ have the following form:

$$d_x^{(1/2)} = \sum_{n=1}^{3} \frac{2J'}{9}\sqrt{1-\frac{(g_z h^z)^2}{J'^2}}\cos(\varphi+\alpha_n)(2-\cos(\boldsymbol{\delta}_n\boldsymbol{k}))$$

$$d_y^{(1/2)} = \sum_{n=1}^{3} \frac{2J'}{9}\sqrt{1-\frac{(g_z h^z)^2}{J'^2}}\sin(\varphi+\alpha_n)(2-\cos(\boldsymbol{\delta}_n\boldsymbol{k}))$$

$$d_z^{(1/2)} = \sum_{n=1}^{3} -\frac{2g_z h^z}{9}(\cos(\boldsymbol{\delta}_n\boldsymbol{k})+1) + \frac{\sqrt{3}}{9}J'\sin(\boldsymbol{\delta}_n\boldsymbol{k}) \tag{12}$$

$$\Delta^{(1/2)} = \sum_{n=1}^{3} \frac{J'}{9} - \frac{\sqrt{3}}{3}D + \frac{\sqrt{3}}{18}g_z h^z \sin(\boldsymbol{\delta}_n\boldsymbol{k}). \tag{13}$$

The translations $\boldsymbol{\delta}_n$, $(n=1,2,3)$ take the previously defined values, and the corresponding phases $\alpha_1=0$, $\alpha_2=-\frac{2\pi}{3}$, and $\alpha_3=\frac{2\pi}{3}$ reflect the Kitaev-type directional dependence of the effective intertrimer interaction also discussed in Ref. [22]. We recall that $\varphi=-5\pi/6$.

To see whether there is a topological transition in the doublet bands via closing and reopening the gap, we need to solve $\boldsymbol{d}_{\mathbf{k}}^{(1/2)}=0$. This is satisfied at the K/K' points for field values $h_{\mathrm{c}}^{(1/2)} = \pm\frac{3J'}{2g_z}$. Therefore, at h_c, a band touching topological transition would occur at the K/K' points. However, h_c is larger than h_{pl}, therefore the spin-1/2 multiplet remains topologically nontrivial all the way to the phase transition into the 1/3-plateau phase.

The high-energy quartet splits too when the magnetic field is finite and the four bands become topologically nontrivial. The surface traced out by $\boldsymbol{d}_{\mathbf{k}}^{(3/2)}$ is similar to what we found for the doublet, but here the orientation is reversed as illustrated with the reversed colors in Fig. 4. The extent of this surface is smaller. Consequently, the band touching topological transition occurs at lower magnetic fields, before the phases transition to the 1/3-plateau phase takes place. The explicit forms of $\boldsymbol{d}_{\mathbf{k}}^{(3/2)}$ and $\Delta_{\mathbf{k}}^{(3/2)}$ are

$$d_x^{(3/2)} = \sum_{j=1}^{3} -\tfrac{J'}{9}\sqrt{1-\tfrac{(g_z h^z)^2}{J'^2}}\cos(\varphi-\alpha_n)(1+\cos(\boldsymbol{\delta}_n\boldsymbol{k}))$$

$$d_y^{(3/2)} = \sum_{j=1}^{3} -\tfrac{J'}{9}\sqrt{1-\tfrac{(g_z h^z)^2}{J'^2}}\sin(\varphi-\alpha_n)(1+\cos(\boldsymbol{\delta}_n\boldsymbol{k}))$$

$$d_z^{(3/2)} = \sum_{j=1}^{3} -\frac{g_z h^z}{18}(4+\cos(\boldsymbol{\delta}_n\boldsymbol{k})) - \frac{\sqrt{3}}{18}J'\sin(\boldsymbol{\delta}_n\boldsymbol{k}) \tag{14}$$

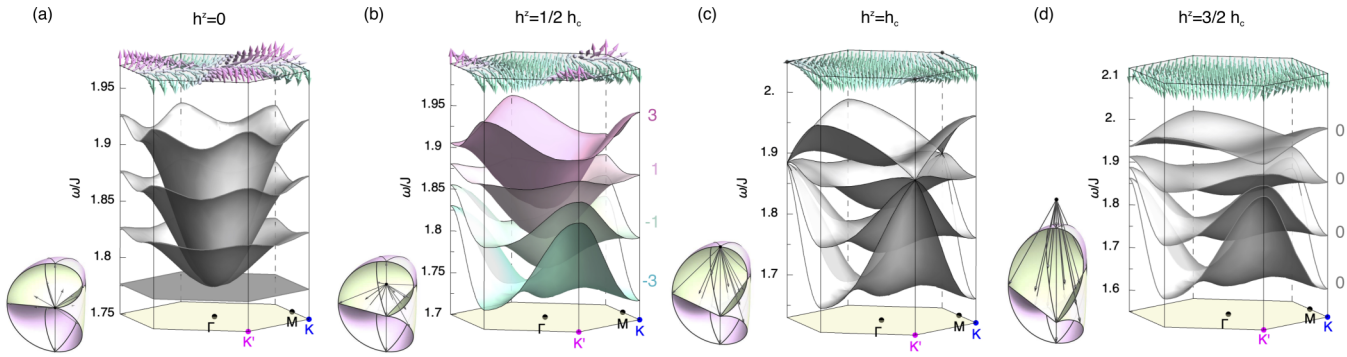

FIG. 4. Topological band touching transition in the quartet subspace. Next to the dispersions we show the surface formed by the pseudofield $\boldsymbol{\delta}_{\mathbf{k}}$. For better understanding, we cut them in halves, to reveal the inside chambers and the position of the origin. (a) At zero field there is quadratic touching at the Γ point. For $0 < h^z < h_c$ fields (b) the bands become fully split and the Chern number is a well defined quantity with the values $2m = 3, 1, -1, -3$. (c) At the critical field, $h^z = h_c$, the bands undergo a band-touching topological transition which takes place at the K' and K points for $h^z = \frac{3J'}{7g_z}$ and $h^z = -\frac{3J'}{7g_z}$, respectively. (d) Above h_c the quartet excitations become topologically trivial. For more information about the skyrmion of $\boldsymbol{\delta}_{\mathbf{k}}$ see Appendix D ($J = 1$, $J' = 0.2$, $D_z = -0.3$, and $g_z = 2$).

$$\Delta^{(3/2)} = \sum_{j=1}^{3} \frac{J}{2} - \frac{\sqrt{3}}{6} D + J' \frac{4 - 3\cos(\boldsymbol{\delta}_n \boldsymbol{k})}{36} - \frac{\sqrt{3} g_z h^z \sin(\boldsymbol{\delta}_n \boldsymbol{k})}{12} \tag{15}$$

with Kitaev-type directional dependent hopping similar to the case of the low-energy doublet subspace.

Solving $\boldsymbol{d}_{\mathbf{k}}^{(3/2)} = \mathbf{0}$, we get a critical field $h_c^{(3/2)} = \pm\frac{3J'}{7g_z}$ at which the topologically nontrivial bands form a novel spin-3/2 Dirac cone with four bands touching at the K/K' point in the BZ as shown in Fig. 4(c). Above $h_c^{(3/2)}$ the gap opens again, and the bands become topologically trivial. The vectors $\boldsymbol{d}_{\mathbf{k}}^{(3/2)}$ too form a skyrmion in the BZ with positive or negative flux for $-\frac{3J'}{7g_z} < h^z < 0$ and $0 < h^z < \frac{3J'}{7g_z}$ field values, respectively. The band-touching transition of the spin-3/2 bands is shown in Fig. 4. Appendices B and C contain details on the derivation of the pseudofields $\boldsymbol{d}_{\mathbf{k}}^{(S)}$ and Appendix D on the skyrmions.

C. Multipolar edge states

The topological nature of bands can be shown through the appearance of edge states in an open system. As an example, we take periodic boundaries along the x direction and open boundaries in the y direction. The multiplet bands for this mixed boundary configuration are plotted in Figs. 5 and 6 together with the recovered bulk bands indicated with colored regions.

In the stripe geometry, we find edge states in the bulk gap connecting the topologically nontrivial bands. To illustrate that these in-gap states are localized on the edges, we plot their exponential decay into the bulk in Fig. 5(b) for the doublet. In this case, there are two edge modes; one on each side, carrying only dipolar degrees of freedom, permitted for a $S = 1/2$.

The local Hilbert space of the spin-3/2 quartet allows for higher order multiplets, such as quadrupole and octupole degrees of freedom. Thus, these multipole characters are naturally present in the quartet bulk bands, furthermore, they promote the emergence of novel multipolar edge modes in finite geometries. To illustrate this, in Fig. 6(b) we plotted the representation of spin-component distribution for two given edge states indicated by the points L and R in Fig. 6(a). The spin coherent state for a spin S can be written as

$$|\boldsymbol{\Omega}\rangle = \sum_{m=-S}^{S} e^{-im\varphi} \sqrt{\binom{2S}{S+m}} \cos^{(S+m)}\frac{\vartheta}{2} \sin^{(S-m)}\frac{\vartheta}{2} |m\rangle \tag{16}$$

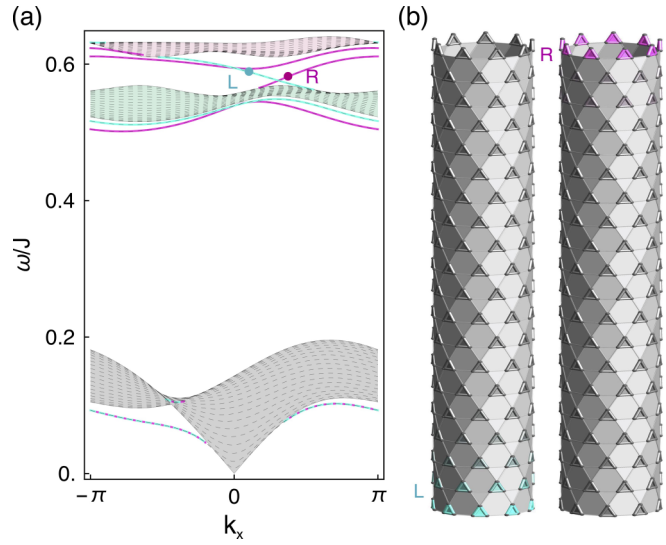

FIG. 5. Edge states appearing in an open system. The lattice has finite width in the y direction and is periodic in the x direction. (a) In the topological regime, in-gap edge states appear connecting the nontrivial bands of the low-energy part. The projection of the bulk bands onto the k_x axis is represented by colored regions. The edge states connecting the Chernful bands are colored according to which side of the stripe they are localized at. Panel (b) illustrates the exponential decay of the edge modes into the bulk with the same color coding to distinguish the localization on opposite sides of the system at given energies as indicated in (a) with the points L and R. The magnetic field is $h^z = h_{\mathrm{pl}}/4$ and the width of the stipe is 20 triangles.

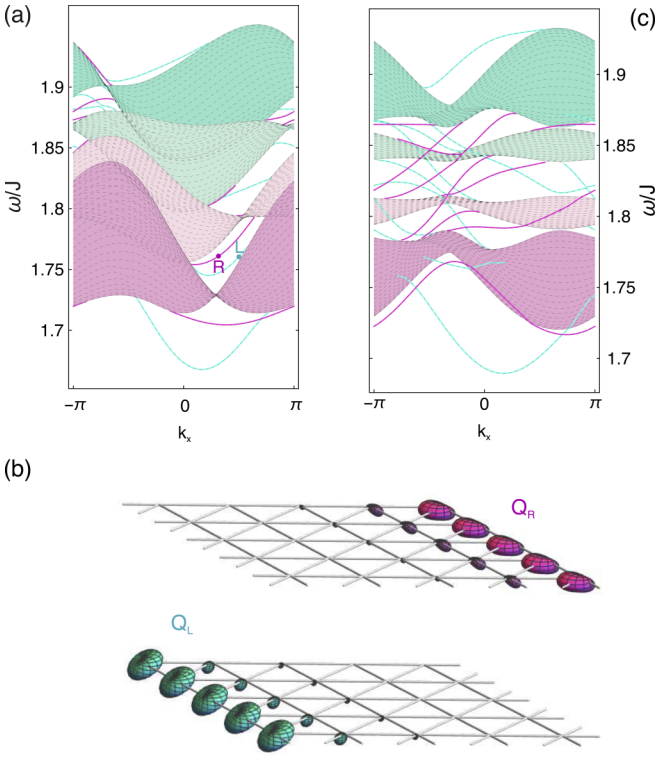

FIG. 6. Edge states in the high-energy quartet at $h^z = h_{\rm pl}/4$. The lattice is open in the y and periodic in the x direction. (b) Spin polarized representation of the representative states R and L. The multipole degrees of freedom allowed by the larger Hilbert space of the $S = 3/2$ quartet is naturally present in the edge states as well. For example, the two modes, R and L, correspond to predominantly quadrupolar excitations traveling on the right (Q_R) and left (Q_L) edges, respectively. The projection of the bulk bands is again represented by colored regions. Due to the 'overlap' of the projected bands, it is difficult to keep track of the edge modes. To be able to see them we flatten the bands by continuously changing the model's parameters so that the topology is not affected as shown in panel (c). We count 3, 4, and 3 modes on each side of the system in the three gaps separating the Chern bands.

and the spin-component distribution of state $|\Psi\rangle$ corresponds to the amplitude $|\langle\mathbf{\Omega}|\Psi\rangle|^2$. In the stripe geometry the basis corresponds to $(\Psi_{1,k_x}, \Psi_{2,k_x}, \ldots, \Psi_{w,k_x})$, where w is the finite width in the y direction. The Ψ_{j,k_x} represents a state in the four-dimensional local Hilbert space of the jth spin 3/2. In Fig. 6(b) the amplitudes $|\langle\mathbf{\Omega}|\Psi_{j,k_x}\rangle|^2$ are plotted for a selected k_x point in the BZ to show not only the weight distribution of the edge states but also their spin-component distribution. The representative edge mode in Fig. 6 has predominantly quadrupolar character. Thus, this in-gap mode corresponds to a spin-quadrupole state [23].

In order to keep account of the edge states appearing in the quartet subspace we flattened the bands by changing parameters in the model in a way that the gaps do not close and the topology is not altered. When the bands are not covering each other, as shown in Fig. 6(c), we can count the edge states. In the three gaps separating the four bands we find 3, 4, and 3 edge states on the left side with negative velocities and the same number of edge states on the right side with positive velocities, in agreement with the Chern numbers, 3, 1, −1, and −3, corresponding to total Chern numbers 3, 4, and 3 in the first, second, and third gap, respectively.

We also find edge states in the topologically trivial regime, $h_z > h_c$, due to the finite geometry. However, these are trivial edge modes that do not collapse the gap by connecting bands, as the edge modes in the nontrivial case do. Instead they begin and end in the same band.

IV. DISCUSSION

In summary, we studied a relevant spin model of the trimerized kagome lattice taking the entangled trimers as building units. The larger local Hilbert space characterizing the trimers naturally allows for multiplet excitations. As a result, an effective spin-1/2 and spin-3/2 band is formed above the gapless magnon mode.

In the chiral magnetic state a small magnetic field removes the degeneracy of the multiplets and the excitations become topologically nontrivial with Chern numbers $C_m = 2m$. Increasing the magnetic field, the bands of the quartet undergo a topological transition when a spin-3/2 Dirac cone is formed by the touching of four bands. Above the critical field the bands become trivial. In case of strong anisotropies, before a similar topological transition occurred for the lower spin-1/2 doublet, a conventional phase transition takes place to the 1/3-plateau phase, in which all bands are topologically trivial. The spin-1/2 doublet carries only dipolar degrees of freedom, providing an analog to the topological insulator formed by itinerant electrons. The spin-3/2 quartet, on the other hand, encompasses higher multipolar characters which in the topologically nontrivial regime is manifested in novel multipolar edge states.

Topologically robust edge states traveling unimpeded at the boundaries are appealing for low-energy consuming fast spintronical devices. Multipolar edge states, put forward here, may be the stepping stone for new directions in these endeavors. A quadrupolar edge mode, for example, can couple to electric field and open a new route towards electric access and control of edge states emerging in the excitation spectrum of magnetic insulators.

We expect that multipolar topological edge modes are present in a broad family of two-dimensional insulating quantum magnets, where the magnetic units are formed by larger spins or entangled dimers or plaquettes. When the propagating spin-S excitations acquire nontrivial topology, due to their multiplet properties, they exhibit novel spin-S Dirac cones and large $-2S, \ldots, 2S$ Chern numbers. Correspondingly, in open systems, chiral edge states emerge with inherent multipolar characters.

ACKNOWLEDGMENTS

The author is gratefully acknowledging discussions with Ludovic Jaubert, Karim Essafi, Nic Shannon, and Karlo Penc. This work was supported by the Theory of Quantum Matter Unit of the Okinawa Institute of Science and Technology Graduate University (OIST) and the Hungarian NKFIH Grant No. K124176.

TABLE I. The multiplet basis suitable for the model Hamiltonian (1). S and m characterize the SU(2) multiplet and its z component. $\chi = \mathbf{S}_1 \cdot (\mathbf{S}_2 \times \mathbf{S}_3)$ and $\chi_v^z = \mathbf{S}_1 \times \mathbf{S}_2 + \mathbf{S}_2 \times \mathbf{S}_3 + \mathbf{S}_3 \times \mathbf{S}_1$ are the scalar and vector chirality, respectively, and $\omega = \frac{2\pi}{3}$. This basis diagonalizes the intratrimer part, and one of the four states, $|S = \frac{1}{2}, m, \chi_v^z\rangle$ with $m = \pm\frac{1}{2}$ and $\chi_v^z = \pm$, is selected as a unique ground state depending on the signs of h^z and D.

SU(2)	S	m	χ	χ_v^z	Basis states
$\mathcal{D}^{(1/2)}$	$\frac{1}{2}$	$\frac{1}{2}$	+	+	$-\frac{\lvert\downarrow\uparrow\uparrow\rangle+e^{i\omega}\lvert\uparrow\downarrow\uparrow\rangle+e^{-i\omega}\lvert\uparrow\uparrow\downarrow\rangle}{\sqrt{3}}$
		$-\frac{1}{2}$	+	−	$\frac{\lvert\uparrow\downarrow\downarrow\rangle+e^{i\omega}\lvert\downarrow\uparrow\downarrow\rangle+e^{-i\omega}\lvert\downarrow\downarrow\uparrow\rangle}{\sqrt{3}}$
$\mathcal{D}^{(1/2)}$	$\frac{1}{2}$	$\frac{1}{2}$	−	−	$\frac{\lvert\downarrow\uparrow\uparrow\rangle+e^{-i\omega}\lvert\uparrow\downarrow\uparrow\rangle+e^{i\omega}\lvert\uparrow\uparrow\downarrow\rangle}{\sqrt{3}}$
		$-\frac{1}{2}$	−	+	$-\frac{\lvert\uparrow\downarrow\downarrow\rangle+e^{-i\omega}\lvert\downarrow\uparrow\downarrow\rangle+e^{i\omega}\lvert\downarrow\downarrow\uparrow\rangle}{\sqrt{3}}$
$\mathcal{D}^{(3/2)}$	$\frac{3}{2}$	$\frac{3}{2}$	0	0	$\lvert\uparrow\uparrow\uparrow\rangle$
		$\frac{1}{2}$	0	0	$\frac{\lvert\downarrow\uparrow\uparrow\rangle+\lvert\uparrow\downarrow\uparrow\rangle+\lvert\uparrow\uparrow\downarrow\rangle}{\sqrt{3}}$
		$-\frac{1}{2}$	0	0	$\frac{\lvert\uparrow\downarrow\downarrow\rangle+\lvert\downarrow\uparrow\downarrow\rangle+\lvert\downarrow\downarrow\uparrow\rangle}{\sqrt{3}}$
		$-\frac{3}{2}$	0	0	$\lvert\downarrow\downarrow\downarrow\rangle$

APPENDIX A: GROUND STATE PROPERTIES AND MULTIPLET BASIS

We collected the multiplet basis that diagonalizes the intratrimer Hamiltonian in Table I. For finite magnetic field and DM interaction all degeneracy is lifted, and the ground state of the strong triangle is uniquely determined by the signs of the field h^z and D.

We choose $D < 0$ that favors the states with positive z component of vector chirality. When the magnetic field is zero the lowest state of the trimer plaquette is twofold degenerate; $|S = \frac{1}{2}, \frac{1}{2}, +\rangle$ and $|S = \frac{1}{2}, -\frac{1}{2}, +\rangle$. Including the intertrimer Heisenberg interaction, the ground state can be described as a general linear combination within this two-dimensional subspace:

$$\cos\vartheta \left|\tfrac{1}{2}, \tfrac{1}{2}, +\right\rangle + e^{i\varphi} \sin\vartheta \left|\tfrac{1}{2}, -\tfrac{1}{2}, +\right\rangle. \tag{A1}$$

The trimer-factorized mean-field energy is given in Eq. (4) in the main text. It only depends on the parameter ϑ and is independent of the phase φ. This freedom in choosing φ reflects the remaining U(1) symmetry of the system after the inclusion of DM interaction. Minimizing Eq. (4), we get $\vartheta = \frac{1}{2}\arccos\frac{g_z h^z}{J'}$. The spins form a 120° order that is canted out of the plane depending on the parameter ϑ. At zero field $\vartheta = \frac{\pi}{4}$, the states mix equally and the spins lie in the lattice plane, while at the critical field $h_c = J/g_z$, $\vartheta = 0$ and a plateau phase is realized as the ground state with $m/m_{\text{sat}} = 1/3$. For convenience we choose $\varphi = -5\pi/6$. The spin expectation values then have the form of

$$\begin{aligned}
\boldsymbol{S}_1 &= \left(-\frac{1}{2\sqrt{3}}\sin 2\vartheta, -\frac{1}{6}\sin 2\vartheta, \frac{1}{6}\cos 2\vartheta\right)\\
\boldsymbol{S}_2 &= \left(\frac{1}{2\sqrt{3}}\sin 2\vartheta, -\frac{1}{6}\sin 2\vartheta, \frac{1}{6}\cos 2\vartheta\right)\\
\boldsymbol{S}_3 &= \left(0, \frac{1}{3}\sin 2\vartheta, \frac{1}{6}\cos 2\vartheta\right)
\end{aligned} \tag{A2}$$

TABLE II. Directional dependence of the neighboring bonds. Depending on the direction of the hopping process, the hopping amplitude acquires a phase factor $e^{i\alpha_n}$ introducing a Kitaev-like degrees of freedom. The bond $(i - j)$ denotes the site indices of the given bond $\boldsymbol{S}_{\mathbf{r},i} \cdot \boldsymbol{S}_{\mathbf{r}+\boldsymbol{\delta}_n,j}$.

n	Bond	$\boldsymbol{\delta}_n$	α_n
1	(2-3)	$\boldsymbol{\delta}_1 = \boldsymbol{\delta}_b - \boldsymbol{\delta}_a$	0
2	(3-1)	$\boldsymbol{\delta}_2 = \boldsymbol{\delta}_a$	$-\frac{2\pi}{3}$
3	(1-2)	$\boldsymbol{\delta}_3 = -\boldsymbol{\delta}_b$	$\frac{2\pi}{3}$

which correspond to the above described 120° order which is canted out of the plane with $S_i^z = \frac{1}{6}\cos 2\vartheta$. In the main text we use $|\text{⁂}\rangle$ to denote this state. The state orthogonal to Eq. (A1) plays the role of a pseudospin flip. It has the form

$$\sin\vartheta \left|\tfrac{1}{2}, \tfrac{1}{2}, +\right\rangle - e^{i\varphi}\cos\vartheta \left|\tfrac{1}{2}, -\tfrac{1}{2}, +\right\rangle, \tag{A3}$$

and spin expectation values similar to Eq. (A2) with opposite signs corresponding to an all-in 120° configuration canted out of the plane with $S_i^z = -\frac{1}{6}\cos 2\vartheta$. Therefore, in the main text we use the notation $|\text{⁂}\rangle$ to refer to this state.

The lowest excitation can be envisaged as the creation of this all-in state and its propagation on the lattice. As discussed in the main text, we introduce a boson to create such pseudospin flip: $a_j^\dagger|0\rangle$, where $|0\rangle$ corresponds to the ground state, i.e., the condensation of $|\text{⁂}\rangle$ which is the vacuum of the all-in triangles. We consider $|\text{⁂}\rangle$ and $|\text{⁂}\rangle$ as the two components of a pseudo spin-half and project the original Hamiltonian (1) onto this two-dimensional subspace. Using the well-known Holstein-Primakoff transformation, we write up the spin wave Hamiltonian of the $a_j^\dagger$ boson that creates the excitation $|\text{⁂}\rangle$.

$$\begin{aligned}
\mathcal{H}^{\text{SW}} = &\sum_{\mathbf{r}} g_z h^z \cos 2\vartheta\, a_{\mathbf{r}}^\dagger a_{\mathbf{r}}\\
&+ \sum_{\mathbf{r}}\sum_{n=1}^{3} \frac{J'}{36}(1 - 2\cos 4\vartheta)(a_{\mathbf{r}}^\dagger a_{\mathbf{r}} + a_{\mathbf{r}+\boldsymbol{\delta}_n}^\dagger a_{\mathbf{r}+\boldsymbol{\delta}_n})\\
&+ \sum_{\mathbf{r}}\sum_{n=1}^{3} \frac{J'}{72}(-5 + i8\sqrt{3}\cos 2\vartheta - 3\cos 4\vartheta) a_{\mathbf{r}}^\dagger a_{\mathbf{r}+\boldsymbol{\delta}_n}\\
&+ \text{H.c.}\\
&+ \sum_{\mathbf{r}}\sum_{n=1}^{3} \frac{J'}{12}\sin^2(2\vartheta) a_{\mathbf{r}}^\dagger a_{\mathbf{r}+\boldsymbol{\delta}_n}^\dagger + \text{H.c.}
\end{aligned} \tag{A4}$$

The position vector $\mathbf{r}$ runs over the unit cells and the translation vectors $\boldsymbol{\delta}_n$ can take the values listed in Table II below and shown in Fig. 1 in the main text. After Fourier transformation we retain the spin wave Hamiltonian Eq. (6) of the main text which can be easily diagonalized using Bogoliubov transformation.

APPENDIX B: EFFECTIVE 2 BY 2 HOPPING MATRIX FOR THE SPIN-HALF MULTIPLET

Here we show the main steps for deriving the effective hopping Hamiltonian describing the dynamics of the low-lying

doublet: $|\frac{1}{2},+\frac{1}{2},-\rangle$ and $|\frac{1}{2},-\frac{1}{2},-\rangle$. We need to calculate matrix elements of the following form:

$$ {}_i\langle \tfrac{1}{2}, m, -|\mathcal{H}|\tfrac{1}{2}, m', -\rangle_j, \tag{B1}$$

where the site indices i and j are either the same or belong to neighboring up-triangles, and m and m' can take the values $-1/2$, and $1/2$.

We then introduce bosonic operators $|\frac{1}{2}, m, -\rangle_{\mathbf{r}} = b^\dagger_{m,\mathbf{r}}|0\rangle$ for the two states and obtain the projected Hamiltonian to this two-dimensional doublet subspace:

$$\begin{aligned}
\mathcal{H}^{(1/2)} = &\sum_{\mathbf{r}}\left[(-\sqrt{3}D - g_z h^z \sin^2\vartheta) b^\dagger_{\frac{1}{2},\mathbf{r}} b_{\frac{1}{2},\mathbf{r}} + (-\sqrt{3}D + g_z h^z \cos^2\vartheta) b^\dagger_{-\frac{1}{2},\mathbf{r}} b_{-\frac{1}{2},\mathbf{r}}\right] \\
&+ \frac{1}{18}\sum_{\mathbf{r}}\sum_{n}\Big[\sin^2\vartheta(2+3\cos 2\vartheta)\left(b^\dagger_{\frac{1}{2},\mathbf{r}} b_{\frac{1}{2},\mathbf{r}} + b^\dagger_{\frac{1}{2},\mathbf{r}+\boldsymbol{\delta}_n} b_{\frac{1}{2},\mathbf{r}+\boldsymbol{\delta}_n}\right) \\
&+ \cos^2\vartheta(2-3\cos 2\vartheta)\left(b^\dagger_{-\frac{1}{2},\mathbf{r}} b_{-\frac{1}{2},\mathbf{r}} + b^\dagger_{-\frac{1}{2},\mathbf{r}+\boldsymbol{\delta}_n} b_{-\frac{1}{2},\mathbf{r}+\boldsymbol{\delta}_n}\right)\Big] \\
&+ \sum_{\mathbf{r}}\sum_{n}\frac{1}{36}\left[(i\sqrt{3} + (i\sqrt{3}-2)\cos 2\vartheta) b^\dagger_{\frac{1}{2},\mathbf{r}} b_{\frac{1}{2},\mathbf{r}+\boldsymbol{\delta}_n} + (-i\sqrt{3} + (i\sqrt{3}+2)\cos 2\vartheta) b^\dagger_{-\frac{1}{2},\mathbf{r}} b_{-\frac{1}{2},\mathbf{r}+\boldsymbol{\delta}_n}\right] + \text{H.c.} \\
&+ \sum_{\mathbf{r}}\sum_{n}\frac{1}{9} e^{-i\varphi} e^{-i\alpha_n} \sin 2\vartheta \left(b^\dagger_{\frac{1}{2},\mathbf{r}} b_{-\frac{1}{2},\mathbf{r}} + b^\dagger_{\frac{1}{2},\mathbf{r}+\boldsymbol{\delta}_n} b_{-\frac{1}{2},\mathbf{r}+\boldsymbol{\delta}_n}\right) + \text{H.c.} \\
&- \sum_{\mathbf{r}}\sum_{n}\frac{1}{18} e^{-i\varphi} e^{-i\alpha_n} \sin 2\vartheta \left(b^\dagger_{\frac{1}{2},\mathbf{r}} b_{-\frac{1}{2},\mathbf{r}+\boldsymbol{\delta}_n} + b^\dagger_{\frac{1}{2},\mathbf{r}+\boldsymbol{\delta}_n} b_{-\frac{1}{2},\mathbf{r}}\right) + \text{H.c.},
\end{aligned} \tag{B2}$$

where $\mathbf{r}$ runs over the unit cells, and the sum for n accounts for the three different directions of the three neighboring triangles. Due to the phase factor, $e^{-i\alpha_n}$, the hopping to the neighbors in the various directions is different, similarly to the Kitaev model. The bonds of different directions, and the corresponding translations, $\boldsymbol{\delta}_n$ and phase factors, α_n are collected in Table II.

After Fourier transformation, we can rewrite Eq. (B2) as a two-by-two problem in the basis $(b^\dagger_{\frac{1}{2},\mathbf{k}}, b^\dagger_{-\frac{1}{2},\mathbf{k}})$:

$$\mathcal{H}^{(1/2)} = \sum_{\mathbf{k}}\sum_{n}\begin{pmatrix} b^\dagger_{\frac{1}{2},\mathbf{k}} \\ b^\dagger_{-\frac{1}{2},\mathbf{k}}\end{pmatrix}\begin{pmatrix} A_{\mathbf{k}} & C_{\mathbf{k}} \\ C^*_{\mathbf{k}} & B_{\mathbf{k}}\end{pmatrix}\begin{pmatrix} b_{\frac{1}{2},\mathbf{k}} \\ b_{-\frac{1}{2},\mathbf{k}}\end{pmatrix}, \tag{B3}$$

where

$$\begin{aligned}
A_{\mathbf{k}} &= \frac{J'}{9} - \frac{\sqrt{3}D}{3} - \frac{g_z h^z}{9}(1+\cos\boldsymbol{\delta}_n\mathbf{k}) + \frac{\sqrt{3}}{18}\sin(\boldsymbol{\delta}_n\mathbf{k})(J' + g_z h^z), \\
B_{\mathbf{k}} &= \frac{J'}{9} - \frac{\sqrt{3}D}{3} + \frac{g_z h^z}{9}(1+\cos\boldsymbol{\delta}_n\mathbf{k}) + \frac{\sqrt{3}}{18}\sin(\boldsymbol{\delta}_n\mathbf{k})(-J' + g_z h^z), \\
C_{\mathbf{k}} &= \frac{J'}{9} e^{-i\varphi} e^{-i\alpha_n}\sqrt{1-\left(\tfrac{g_z h^z}{J'}\right)^2}(2-\cos(\boldsymbol{\delta}_n\mathbf{k}))
\end{aligned} \tag{B4}$$

and we used the variational solution $\vartheta = \frac{1}{2}\arccos\frac{g_z h^z}{J'}$. The independent parameter φ is chosen to be $-5\pi/6$.

We can bring Eq. (B3) to the convenient form $\Delta^{(1/2)}_{\mathbf{k}}\cdot\mathbf{1}_2 + \boldsymbol{d}^{(1/2)}_{\mathbf{k}}\cdot\boldsymbol{s}$, as stated in the main text. The vector $\boldsymbol{s}$ is $\frac{1}{2}\boldsymbol{\sigma}$, with $\boldsymbol{\sigma}$ denoting the Pauli matrices. $\mathbf{1}_2$ is the two-dimensional identity matrix and $\Delta^{(1/2)}_{\mathbf{k}}$ corresponds to the gap of the doublet. The explicit forms of the vector $\boldsymbol{d}^{(1/2)}(\mathbf{k})$ and $\Delta^{(1/2)}_{\mathbf{k}}$ are given in the main text in Eqs. (12) and (13), respectively.

APPENDIX C: EFFECTIVE 4 BY 4 HOPPING OF THE SPIN-3/2 QUARTET

We follow the same steps as in the case of the doublet in Sec. B and project the original problem onto the subspace of $|\frac{3}{2},+\frac{3}{2},0\rangle$ $|\frac{3}{2},+\frac{1}{2},\rangle$, $|\frac{3}{2},-\frac{1}{2},0\rangle$ and $|\frac{3}{2},-\frac{3}{2},0\rangle$. We need to calculate matrix elements of the following form:

$$ {}_i\langle \tfrac{3}{2}, m, 0|\mathcal{H}|\tfrac{3}{2}, m', 0\rangle_j, \tag{C1}$$

where the indices i and j denote the sites of the same or neighboring up-triangles, furthermore m and m' can take the values $-3/2,\ldots,3/2$.

Upon introducing bosonic operators $|\frac{3}{2}, m, 0\rangle_{\mathbf{r}} = c^{\dagger}_{m,\mathbf{r}}|0\rangle$ for the four states we construct the projected hopping Hamiltonian of the quartet subspace: $\mathcal{H}^{(3/2)} = \mathcal{H}^{(3/2)}_{\text{diag}} + \mathcal{H}^{(3/2)}_{\text{off-diag}}$

$$
\begin{aligned}
\mathcal{H}^{(3/2)}_{\text{diag}} = & \sum_{\mathbf{r}} \left[\frac{3J}{2} - \frac{\sqrt{3}D}{2} + \frac{1}{2} g_z h^z \cos 2\vartheta \right] \left(c^{\dagger}_{\frac{3}{2},\mathbf{r}} c_{\frac{3}{2},\mathbf{r}} + c^{\dagger}_{\frac{1}{2},\mathbf{r}} c_{\frac{1}{2},\mathbf{r}} + c^{\dagger}_{-\frac{1}{2},\mathbf{r}} c_{-\frac{1}{2},\mathbf{r}} + c^{\dagger}_{-\frac{3}{2},\mathbf{r}} c_{-\frac{3}{2},\mathbf{r}} \right) \\
& + \sum_{\mathbf{r}} g_z h^z \left[-\frac{3}{2} c^{\dagger}_{\frac{3}{2},\mathbf{r}} c_{\frac{3}{2},\mathbf{r}} - \frac{1}{2} c^{\dagger}_{\frac{1}{2},\mathbf{r}} c_{\frac{1}{2},\mathbf{r}} + \frac{1}{2} c^{\dagger}_{-\frac{1}{2},\mathbf{r}} c_{-\frac{1}{2},\mathbf{r}} + \frac{3}{2} c^{\dagger}_{-\frac{3}{2},\mathbf{r}} c_{-\frac{3}{2},\mathbf{r}} \right] \\
& + \frac{1}{72} \sum_{\mathbf{r}} \sum_{n} (1 + 6\cos 2\vartheta - 3\cos 4\vartheta) \left(c^{\dagger}_{\frac{3}{2},\mathbf{r}} c_{\frac{3}{2},\mathbf{r}} + c^{\dagger}_{\frac{3}{2},\mathbf{r}+\boldsymbol{\delta}_n} c_{\frac{3}{2},\mathbf{r}+\boldsymbol{\delta}_n} \right) \\
& + \frac{1}{18} \sum_{\mathbf{r}} \sum_{n} (2 + 3\cos 2\vartheta) \sin^2 \vartheta \left(c^{\dagger}_{\frac{1}{2},\mathbf{r}} c_{\frac{1}{2},\mathbf{r}} + c^{\dagger}_{\frac{1}{2},\mathbf{r}+\boldsymbol{\delta}_n} c_{\frac{1}{2},\mathbf{r}+\boldsymbol{\delta}_n} \right) \\
& + \frac{1}{18} \sum_{\mathbf{r}} \sum_{n} (2 - 3\cos 2\vartheta) \cos^2 \vartheta \left(c^{\dagger}_{-\frac{1}{2},\mathbf{r}} c_{-\frac{1}{2},\mathbf{r}} + c^{\dagger}_{-\frac{1}{2},\mathbf{r}+\boldsymbol{\delta}_n} c_{-\frac{1}{2},\mathbf{r}+\boldsymbol{\delta}_n} \right) \\
& + \frac{1}{72} \sum_{\mathbf{r}} \sum_{n} (1 - 6\cos 2\vartheta - 3\cos 4\vartheta) \left(c^{\dagger}_{-\frac{3}{2},\mathbf{r}} c_{-\frac{3}{2},\mathbf{r}} + c^{\dagger}_{-\frac{3}{2},\mathbf{r}+\boldsymbol{\delta}_n} c_{-\frac{3}{2},\mathbf{r}+\boldsymbol{\delta}_n} \right) \\
& + \frac{1}{6} \sum_{\mathbf{r}} \sum_{n} \left[\cos^2 \vartheta e^{-i\frac{2\pi}{3}} c^{\dagger}_{\frac{3}{2},\mathbf{r}} c_{\frac{3}{2},\mathbf{r}+\boldsymbol{\delta}_n} + \sin^2 \vartheta e^{i\frac{2\pi}{3}} c^{\dagger}_{-\frac{3}{2},\mathbf{r}} c_{-\frac{3}{2},\mathbf{r}+\boldsymbol{\delta}_n} + \text{H.c.} \right] \\
& + \frac{1}{72} \sum_{\mathbf{r}} \sum_{n} [(-3 - \cos 2\vartheta) + i\sqrt{3}(-1 - 3\cos 2\vartheta)] c^{\dagger}_{\frac{1}{2},\mathbf{r}} c_{\frac{1}{2},\mathbf{r}} + \text{H.c.} \\
& + \frac{1}{72} \sum_{\mathbf{r}} \sum_{n} [(-3 + \cos 2\vartheta) + i\sqrt{3}(1 - 3\cos 2\vartheta)] c^{\dagger}_{-\frac{1}{2},\mathbf{r}} c_{-\frac{1}{2},\mathbf{r}+\boldsymbol{\delta}_n} + \text{H.c.}
\end{aligned} \tag{C2}
$$

$$
\begin{aligned}
\mathcal{H}^{(3/2)}_{\text{off-diag}} = & \frac{\sqrt{3}}{18} \sum_{\mathbf{r}} \sum_{n} e^{-i\varphi} e^{i\alpha_n} \sin 2\vartheta \left[e^{i\frac{2\pi}{3}} c^{\dagger}_{\frac{3}{2},\mathbf{r}} c_{\frac{1}{2},\mathbf{r}} + e^{-i\frac{2\pi}{3}} c^{\dagger}_{\frac{3}{2},\mathbf{r}+\boldsymbol{\delta}_n} c_{\frac{1}{2},\mathbf{r}+\boldsymbol{\delta}_n} \right] + \text{H.c.} \\
& + \frac{1}{9} \sum_{\mathbf{r}} \sum_{n} e^{-i\varphi} e^{i\alpha_n} \sin 2\vartheta \left[e^{i\frac{2\pi}{3}} c^{\dagger}_{\frac{1}{2},\mathbf{r}} c_{-\frac{1}{2},\mathbf{r}} + e^{-i\frac{2\pi}{3}} c^{\dagger}_{\frac{1}{2},\mathbf{r}+\boldsymbol{\delta}_n} c_{-\frac{1}{2},\mathbf{r}+\boldsymbol{\delta}_n} \right] + \text{H.c.} \\
& + \frac{\sqrt{3}}{18} \sum_{\mathbf{r}} \sum_{n} e^{-i\varphi} e^{i\alpha_n} \sin 2\vartheta \left[e^{i\frac{2\pi}{3}} c^{\dagger}_{-\frac{1}{2},\mathbf{r}} c_{-\frac{3}{2},\mathbf{r}} + e^{-i\frac{2\pi}{3}} c^{\dagger}_{-\frac{1}{2},\mathbf{r}+\boldsymbol{\delta}_n} c_{-\frac{3}{2},\mathbf{r}+\boldsymbol{\delta}_n} \right] + \text{H.c.} \\
& - \frac{\sqrt{3}}{36} \sum_{\mathbf{r}} \sum_{n} e^{-i\varphi} e^{i\alpha_n} \sin 2\vartheta \left[c^{\dagger}_{\frac{3}{2},\mathbf{r}} c_{\frac{1}{2},\mathbf{r}+\boldsymbol{\delta}_n} + c^{\dagger}_{\frac{3}{2},\mathbf{r}+\boldsymbol{\delta}_n} c_{\frac{1}{2},\mathbf{r}} \right] + \text{H.c.} \\
& - \frac{1}{18} \sum_{\mathbf{r}} \sum_{n} e^{-i\varphi} e^{i\alpha_n} \sin 2\vartheta \left[c^{\dagger}_{\frac{1}{2},\mathbf{r}} c_{-\frac{1}{2},\mathbf{r}+\boldsymbol{\delta}_n} + c^{\dagger}_{\frac{1}{2},\mathbf{r}+\boldsymbol{\delta}_n} c_{-\frac{1}{2},\mathbf{r}} \right] + \text{H.c.} \\
& - \frac{\sqrt{3}}{36} \sum_{\mathbf{r}} \sum_{n} e^{-i\varphi} e^{i\alpha_n} \sin 2\vartheta \left[c^{\dagger}_{-\frac{1}{2},\mathbf{r}} c_{-\frac{3}{2},\mathbf{r}+\boldsymbol{\delta}_n} + c^{\dagger}_{-\frac{1}{2},\mathbf{r}+\boldsymbol{\delta}_n} c_{-\frac{3}{2},\mathbf{r}} \right] + \text{H.c.}
\end{aligned} \tag{C3}
$$

The translations $\boldsymbol{\delta}_n$ and the phase factors $e^{-i\alpha_n}$ take the values defined in Table II. Similar to the doublet effective model, the hopping to the neighbors has Kitaev-like direction dependence through the phase factor $e^{-i\alpha_n}$.

After Fourier transformation, we can rewrite Eqs. (C3) and (C2) as a four-by-four hopping Hamiltonian in the basis $(c^{\dagger}_{\frac{3}{2},\mathbf{k}}, c^{\dagger}_{\frac{1}{2},\mathbf{k}}, c^{\dagger}_{-\frac{1}{2},\mathbf{k}}, c^{\dagger}_{-\frac{3}{2},\mathbf{k}})$:

$$
\mathcal{H}^{(3/2)} = \sum_{\mathbf{k}} \sum_{n=1}^{3} \begin{pmatrix} c^{\dagger}_{\frac{3}{2},\mathbf{k}} \\ c^{\dagger}_{\frac{1}{2},\mathbf{k}} \\ c^{\dagger}_{-\frac{1}{2},\mathbf{k}} \\ c^{\dagger}_{-\frac{3}{2},\mathbf{k}} \end{pmatrix} \begin{pmatrix} M_{\frac{3}{2},\frac{3}{2}} & M_{\frac{3}{2},\frac{1}{2}} & 0 & 0 \\ M^{*}_{\frac{3}{2},\frac{1}{2}} & M_{\frac{1}{2},\frac{1}{2}} & M_{\frac{1}{2},-\frac{1}{2}} & 0 \\ 0 & M^{*}_{\frac{1}{2},-\frac{1}{2}} & M_{-\frac{1}{2},-\frac{1}{2}} & M_{-\frac{1}{2},-\frac{3}{2}} \\ 0 & 0 & M^{*}_{-\frac{1}{2},-\frac{3}{2}} & M_{-\frac{3}{2},-\frac{3}{2}} \end{pmatrix} \begin{pmatrix} c_{\frac{3}{2},\mathbf{k}} \\ c_{\frac{1}{2},\mathbf{k}} \\ c_{-\frac{1}{2},\mathbf{k}} \\ c_{-\frac{3}{2},\mathbf{k}} \end{pmatrix}, \tag{C4}
$$

where the diagonal terms are

$$
\begin{aligned}
M_{\frac{3}{2},\frac{3}{2}} &= \frac{J}{2} - \frac{D}{2\sqrt{3}} + \frac{J'}{9} - \frac{J'}{12}\cos(\boldsymbol{\delta}_n\mathbf{k}) - \frac{J'}{4\sqrt{3}}\sin(\boldsymbol{\delta}_n\mathbf{k}) - \frac{g_z h^z}{4\sqrt{3}}\sin(\boldsymbol{\delta}_n\mathbf{k}) - \frac{g_z h^z}{12}(4+\cos(\boldsymbol{\delta}_n\mathbf{k})) \\
M_{\frac{1}{2},\frac{1}{2}} &= \frac{J}{2} - \frac{D}{2\sqrt{3}} + \frac{J'}{9} - \frac{J'}{12}\cos(\boldsymbol{\delta}_n\mathbf{k}) - \frac{J'}{12\sqrt{3}}\sin(\boldsymbol{\delta}_n\mathbf{k}) - \frac{g_z h^z}{4\sqrt{3}}\sin(\boldsymbol{\delta}_n\mathbf{k}) - \frac{g_z h^z}{36}(4+\cos(\boldsymbol{\delta}_n\mathbf{k})) \\
M_{-\frac{1}{2},-\frac{1}{2}} &= \frac{J}{2} - \frac{D}{2\sqrt{3}} + \frac{J'}{9} - \frac{J'}{12}\cos(\boldsymbol{\delta}_n\mathbf{k}) + \frac{J'}{12\sqrt{3}}\sin(\boldsymbol{\delta}_n\mathbf{k}) - \frac{g_z h^z}{4\sqrt{3}}\sin(\boldsymbol{\delta}_n\mathbf{k}) + \frac{g_z h^z}{36}(4+\cos(\boldsymbol{\delta}_n\mathbf{k})) \\
M_{-\frac{3}{2},-\frac{3}{2}} &= \frac{J}{2} - \frac{D}{2\sqrt{3}} + \frac{J'}{9} - \frac{J'}{12}\cos(\boldsymbol{\delta}_n\mathbf{k}) + \frac{J'}{4\sqrt{3}}\sin(\boldsymbol{\delta}_n\mathbf{k}) - \frac{g_z h^z}{4\sqrt{3}}\sin(\boldsymbol{\delta}_n\mathbf{k}) + \frac{g_z h^z}{12}(4+\cos(\boldsymbol{\delta}_n\mathbf{k}))
\end{aligned}
\tag{C5}
$$

and the off-diagonal part is given by:

$$
\begin{aligned}
M_{\frac{3}{2},\frac{1}{2}} &= -\frac{J\sqrt{3}}{18}e^{-i\varphi}e^{i\alpha_n}\sin 2\vartheta(1+\cos(\boldsymbol{\delta}_n\mathbf{k})) \\
M_{\frac{1}{2},\frac{1}{2}} &= -\frac{J}{9}e^{-i\varphi}e^{i\alpha_n}\sin 2\vartheta(1+\cos(\boldsymbol{\delta}_n\mathbf{k})) \\
M_{-\frac{1}{2},-\frac{1}{2}} &= -\frac{J\sqrt{3}}{18}e^{-i\varphi}e^{i\alpha_n}\sin 2\vartheta(1+\cos(\boldsymbol{\delta}_n\mathbf{k})).
\end{aligned}
\tag{C6}
$$

The free parameter φ is again $-5\pi/6$ and we need to insert the variational solution, $\frac{1}{2}\arccos\frac{g_z h^z}{J'}$ for ϑ.

We started with a purely spin-spin problem, and no higher order tensors, such as quadrupolar-quadrupolar terms, were taken into account in the original Hamiltonian Eq. (1) defined in the main text. For this reason the effective hopping model contains only spinlike terms, such as spin raising and lowering components and diagonal contributions, but there is no quadrupole or octupole components that were otherwise allowed by the larger Hilbert space of the effective spin-3/2 object. Consequently, the effective hopping model for the quartet (C4) can also be written in the form of $\Delta_{\mathbf{k}}^{(3/2)}\cdot\mathbf{1}_4 + \boldsymbol{d}_{\mathbf{k}}^{(3/2)}\cdot\boldsymbol{S}$, where the $\mathbf{1}_4$ is a four-dimensional identity matrix, and $\boldsymbol{S}$ is the vector constructed from the spin operators of an $S = 3/2$ quantum spin:

$$
S^x = \begin{pmatrix} 0 & \frac{\sqrt{3}}{2} & 0 & 0 \\ \frac{\sqrt{3}}{2} & 0 & 1 & 0 \\ 0 & 1 & 0 & \frac{\sqrt{3}}{2} \\ 0 & 0 & \frac{\sqrt{3}}{2} & 0 \end{pmatrix},\quad
S^y = \begin{pmatrix} 0 & \frac{-i\sqrt{3}}{2} & 0 & 0 \\ \frac{i\sqrt{3}}{2} & 0 & -i & 0 \\ 0 & i & 0 & \frac{-i\sqrt{3}}{2} \\ 0 & 0 & \frac{i\sqrt{3}}{2} & 0 \end{pmatrix},\quad
S^z = \begin{pmatrix} \frac{3}{2} & 0 & 0 & 0 \\ 0 & \frac{1}{2} & 0 & 0 \\ 0 & 0 & -\frac{1}{2} & 0 \\ 0 & 0 & 0 & -\frac{3}{2} \end{pmatrix}.
\tag{C7}
$$

APPENDIX D: THE FORMS OF VECTOR $\boldsymbol{d}_{\mathbf{k}}^{(S)}$ AND THE TRANSITION POINTS

As discussed in the main text the topology of the system is encompassed in the pseudomagnetic fields $\boldsymbol{d}_{\mathbf{k}}^{(S)}$. In Fig. 7 we illustrate this property. Subfigures 7(a), 7(b) and 7(c) belong to the doublet, while 7(c), 7(d), and 7(e) are representatives of the quartet. We plot the surface spanned by $\boldsymbol{d}_{\mathbf{k}}^{(1/2)}$ and $\boldsymbol{d}_{\mathbf{k}}^{(3/2)}$ in Figs. 7(a) and 7(d), respectively, from different point of views to help visualize the shape of the surface. It has a threefold symmetry along the z axis, inherited from the symmetry of the lattice. Furthermore, it encloses two separate chambers. When the origin of the $\boldsymbol{d}_{\mathbf{k}}^{(S)}$ vectors is inside, the bands are fully gapped and the spin-S multiplet is topologically nontrivial with Chern numbers $-2S,\ldots,2S$. In such cases the vectors $\boldsymbol{d}_{\mathbf{k}}^{(S)}$ form a skyrmion in the Brillouin zone (BZ) as shown in Figs. 7(c) and 7(e) for the doublet and quartet. When the origin sits on the surface, a $\boldsymbol{d}_{\mathbf{k}}^{(S)}$ is zero somewhere in the BZ and the bands touch, forming a novel spin-S Dirac cone. Such is the case for example at zero magnetic field shown in Fig. 7(b) for the doublet. In cases when the origin is outside the chambers, the bands are fully gapped and topologically trivial as indicated in Fig. 7(f). This only happens in the case of the quartet. The transition field for the doublet is too high for such a band touching topological transition, and at lower critical field a symmetry breaking phase transition takes place into the 1/3-magnetization plateau phase.

APPENDIX E: VARIATIONAL PHASE DIAGRAM AND MULTIBOSON THEORY FOR ENTANGLED TRIMERS

In this section we derive the multiboson theory for the kagomé antiferromagnet with breathing anisotropy to be able to validate our effective model of the main text in the case of stronger DM and breathing anisotropies. As a first step we determine the variational ground state. For this, we keep the up-triangles quantum mechanically entangled and treat the interaction J' between them on a mean-field level. The variational wave function is trimer-factorized $|\Psi\rangle = \prod_{j\in\triangle}|\psi\rangle_j$, with

$$
|\psi\rangle = \sum_{S,m,\chi_v^z} a_{S,m\chi_v^z}\left|S,m,\chi_v^z\right\rangle,
\tag{E1}
$$

where the complex variational parameters $a_{S,m\chi_v^z}$ are determined by minimizing the energy $E_0 = \frac{\langle\Psi|\mathcal{H}|\Psi\rangle}{\langle\Psi|\Psi\rangle}$. The resulting variational phase diagram is depicted in Fig. 8.

For zero magnetic field the ground state is planar antiferromagnetic state with shortened spins due to local entanglement.

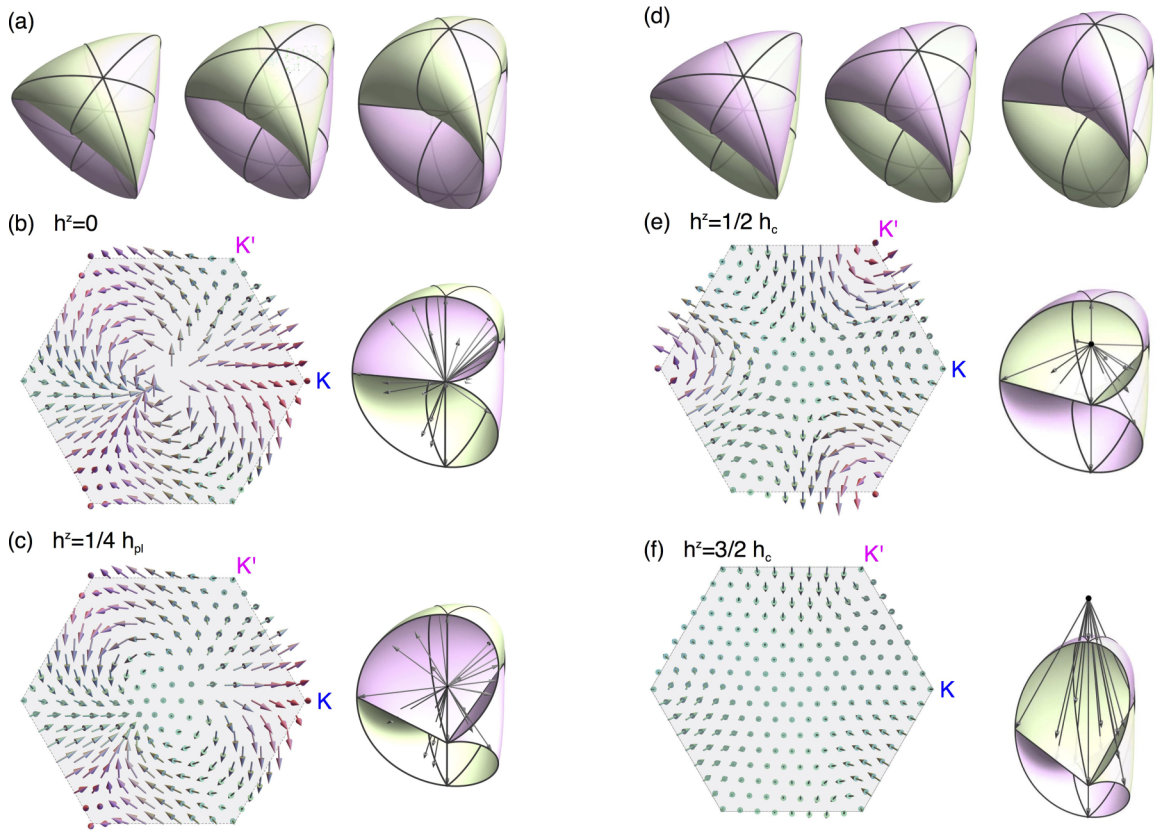

FIG. 7. (a) and (d) show the two-dimensional surface spanned by the vectors $\boldsymbol{d}_{\mathbf{k}}^{(1/2)}$ and $\boldsymbol{d}_{\mathbf{k}}^{(3/2)}$, respectively. The different viewpoints help envisaging the threefold symmetry carried over from the lattice to the vectors $\boldsymbol{d}_{\mathbf{k}}^{(S)}$ and the the two chambers enclosed. When the origin of the vectors is inside one of the chambers, the corresponding multiplet bands are topologically nontrivial and the $\boldsymbol{d}_{\mathbf{k}}^{(S)}$ forms a skyrmion in the Brillouin zone as shown in (c) and (e). If the origin is a part of the surface, necessarily one of the $\boldsymbol{d}_{\mathbf{k}}^{(S)}$ vectors has zero length, and the multiplets are degenerate with undefined Chern numbers, such as the case for zero magnetic field as shown in (b) in the case of the doublet. When the origin is outside of the surface, the bands are fully gapped again, with trivial topology and zero Chern numbers as illustrated in (f) for the quartet.

A finite field cants the spins out of the plane and the chiral magnetic phase is realized, in which the shortened spins form an umbrella similar to the antiferromagnetic phase but with finite z component. At larger values of magnetic field we enter the 1/3-plateau phase. In this entangled phase, the spins are parallel to the z direction, For very small DM interaction and small breathing anisotropy, the plateau is realized by an 'up-up-down' configuration, in which two sites of the triangles are equivalent. A corresponding phase has been found by using tensor network methods [24]. In the case of larger anisotropies, the plateau phase is realized by the spins all pointing in the direction of the field and having $\langle S^z \rangle = 1/6$, instead of the full 1/2 value, as a consequence of quantum mechanical entanglement. When the anisotropies get smaller the uniform phases, namely the saturated and the plateau phase shrink and the chiral phase becomes more extended.

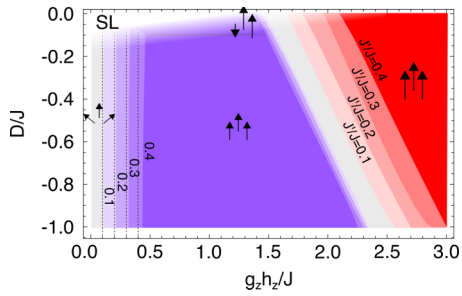

FIG. 8. Variational phase diagram for the Hamiltonian (1) as the function of magnetic field and DM interaction for different values of intertrimer interaction J' denoted by different shades. Lighter colors correspond to smaller values of J'. The magnetic phases shrink as the anisotropies become smaller. In the gray area the chiral magnetic umbrella state is the ground state, characterized with topologically nontrivial multiplet bands. Increasing the magnetic field, we enter the plateau phase with $m/m_{\text{sat}} = 1/3$. In high magnetic fields the saturated phase is realized. The vertical dashed lines correspond to the phase boundary $g_z h_{\text{pl}} = J'/J$ given by the effective model. As expected, for larger anisotropies this value becomes more accurate.

In the case of zero DM interaction and zero magnetic field, the ground state is a more elaborate spin liquid state [22] which is present even for strong breathing anisotropies. The discussion of this phase is beyond the scope of the variational approach used here.

Having determined the ground state, we can construct the additional seven states which are orthogonal to $|\psi\rangle$. After constructing the new rotated basis, we introduce a boson $a_n^\dagger$, $(n = 0, \ldots, 7)$ for each state, and condense $a_0^\dagger$ which creates the ground state from the vacuum, $a_0^\dagger|0\rangle = |\psi\rangle$. The other seven bosons $a_n^\dagger$, $(n = 1, \ldots, 7)$ stand for the excitations. We

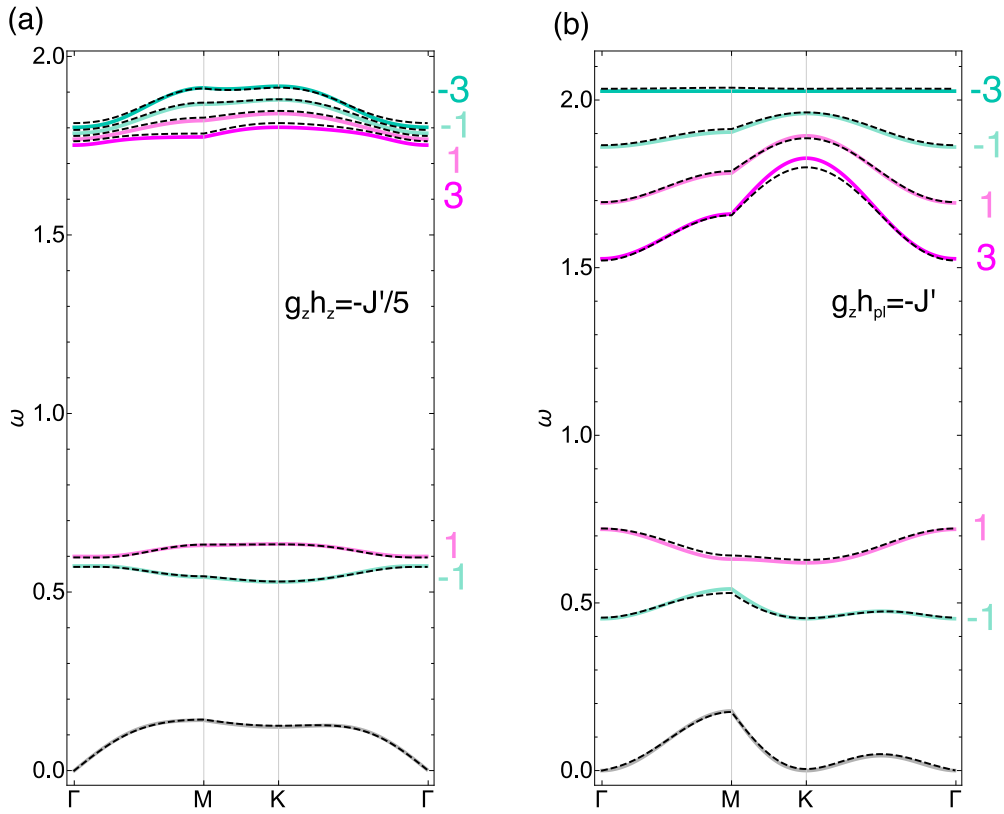

FIG. 9. Comparing the multiboson (dashed black) and effective (solid colored) approaches for the anisotropic case with parameters $J'/J = 0.2$, $D/J = -0.3$ used in the effective model introduced in Sec. III. In panel (a) the magnetic field is small and the ground state corresponds to the chiral magnetic phase. All seven modes are in good agreement with the full multiboson spectrum plotted with a dashed line. (b) Spectra at the border of the plateau phase. The Goldstone mode softens at the K point for $h < 0$. (For $h > 0$ the softening occurs at K′. This softening is evident in Fig. 3 as well). We have a good agreement between the effective model (solid) and the multiboson (dashed) spectrum.

derive the multiboson spin wave Hamiltonian by eliminating $a_0^\dagger$ and a_0 using the constraint

$$\sum_{n=0}^{7} a_n^\dagger a_n = 1 \,. \tag{E2}$$

The multiboson Hamiltonian has the general form

$$\mathcal{H}^{\rm sw} = \begin{pmatrix} \underline{a}_{\mathbf{k}}^\dagger \\ \underline{a}_{-\mathbf{k}} \end{pmatrix} \begin{pmatrix} \mathbf{M}_{\mathbf{k}} & \mathbf{N}_{\mathbf{k}} \\ \mathbf{N}_{-\mathbf{k}}^* & \mathbf{M}_{-\mathbf{k}}^* \end{pmatrix} \begin{pmatrix} \underline{a}_{\mathbf{k}} \\ \underline{a}_{-\mathbf{k}}^\dagger \end{pmatrix} , \tag{E3}$$

where $\underline{a}_{\mathbf{k}}^\dagger$ is a vector of the seven components and $\mathbf{M}_{\mathbf{k}}$ and $\mathbf{N}_{\mathbf{k}}$ are 7 by 7 matrices. The multiboson theory includes matrix elements between the multiplets, as well as the pairing terms such as $a_{n,\mathbf{k}}^\dagger a_{m,-\mathbf{k}}^\dagger$ and $a_{n,-\mathbf{k}} a_{m,\mathbf{k}}$ which are neglected in the effective model introduced in Sec. III for the strongly anisotropic case. To validate our results obtained by the effective approach, we plot the multiboson spectrum for the same parameters used in Sec. III for the small field and for the vicinity of the transition to the plateau phase in Fig. 9. For both field values we find very good agreement for all seven modes, including the Goldstone mode, the doublet, and the quartet excitations. We then numerically calculated the Chern numbers for each band using the method introduced in Ref. [25] and find the same values as in the case of the effective approach.

[1] S. Raghu and F. D. M. Haldane, Phys. Rev. A **78**, 033834 (2008).

[2] A. Petrescu, A. A. Houck, and K. Le Hur, Phys. Rev. A **86**, 053804 (2012).

[3] M. C. Rechtsman, J. M. Zeuner, Y. Plotnik, Y. Lumer, D. Podolsky, F. Dreisow, S. Nolte, M. Segev, and A. Szameit, Nature (London) **496**, 196 (2013).

[4] M. Hafezi, S. Mittal, J. Fan, A. Migdall, and J. M. Taylor, Nat. Photon. **7**, 1001 (2013).

[5] A. B. Khanikaev, S. Hossein Mousavi, W.-K. Tse, M. Kargarian, A. H. MacDonald, and G. Shvets, Nat. Mater. **12**, 233 (2013).

[6] L. Lu, J. D. Joannopoulos, and M. Soljacic, Nat. Photon. **8**, 821 (2014).

[7] L. Zhang, J. Ren, J.-S. Wang, and B. Li, Phys. Rev. Lett. **105**, 225901 (2010).

[8] L. Zhang, J. Ren, J.-S. Wang, and B. Li, J. Phys.: Condens. Matter **23**, 305402 (2011).

[9] T. Qin, J. Zhou, and J. Shi, Phys. Rev. B **86**, 104305 (2012).
[10] K. A. van Hoogdalem, Y. Tserkovnyak, and D. Loss, Phys. Rev. B **87**, 024402 (2013).
[11] W. Jiang, X. Zhang, G. Yu, W. Zhang, X. Wang, M. Benjamin Jungfleisch, J. E. Pearson, X. Cheng, O. Heinonen, K. L. Wang, Y. Zhou, A. Hoffmann, and S. G. E. te Velthuis, Nat. Phys. **13**, 162 (2017).
[12] K. Litzius, I. Lemesh, B. Kruger, P. Bassirian, L. Caretta, K. Richter, F. Buttner, K. Sato, O. A. Tretiakov, J. Forster, R. M. Reeve, M. Weigand, I. Bykova, H. Stoll, G. Schutz, G. S. D. Beach, and M. Klaui, Nat. Phys. **13**, 170 (2017).
[13] H.-S. Kim and H.-Y. Kee, npj Quantum Mater. **2**, 20 (2017).
[14] F.-Y. Li, Y.-D. Li, Y. B. Kim, L. Balents, Y. Yu, and G. Chen, Nat. Commun. **7**, 12691 (2016).
[15] L. Zhang, J. Ren, J.-S. Wang, and B. Li, Phys. Rev. B **87**, 144101 (2013).
[16] R. Chisnell, J. S. Helton, D. E. Freedman, D. K. Singh, R. I. Bewley, D. G. Nocera, and Y. S. Lee, Phys. Rev. Lett. **115**, 147201 (2015).
[17] S. A. Owerre, Phys. Rev. B **97**, 094412 (2018).
[18] J. Romhányi, K. Penc, and R. Ganesh, Nat. Commun. **6**, 6805 (2015).
[19] M. Malki and K. P. Schmidt, Phys. Rev. B **95**, 195137 (2017).
[20] P. A. McClarty, F. Kruger, T. Guidi, S. F. Parker, K. Refson, A. W. Parker, D. Prabhakaran, and R. Coldea, Nat. Phys. **13**, 736 (2017).
[21] V. Subrahmanyam, Phys. Rev. B **52**, 1133 (1995).
[22] C. Repellin, Y.-C. He, and F. Pollmann, Phys. Rev. B **96**, 205124 (2017).
[23] Let us note that an excited state with multipolar degrees of freedom and a multipolar transition should be distinguished. For example, by quadrupolar excitation we mean an excited state exhibiting quadrupole degrees of freedom. This is, however, not necessarily a quadrupolar transition involving the creation of two magnons. Similarly, a quadrupolar transition can lead to a creation of a magnetic excitation, which happens, for example, in the case of a $\Delta S^z = \pm 2$ transition between the magnetic $S^z = 1$ and -1 states of a spin-1.
[24] T. Picot, M. Ziegler, R. Orús, and D. Poilblanc, Phys. Rev. B **93**, 060407 (2016).
[25] T. Fukui, Y. Hatsugai, and H. Suzuki, J. Phys. Soc. Jpn. **74**, 1674 (2005).